Arrival Optimization with Point Merge in a Dual-runway Environment

Henrik Hardell
Communications and Transport Systems, ITN,
Linköping University (LiU), Norrköping, Sweden
Airspace Unit, Luftfartsverket (LFV),
Norrköping, Sweden, henrik.hardell@liu.se

Tatiana Polishchuk, Lucie Smetanová
Communications and Transport Systems, ITN
Linköping University (LiU)
Norrköping, Sweden
firstname.lastname@liu.se

***Abstract*—We present an application of a mixed-integer programming framework, for an automated scheduling and deconfliction of the arriving and departing traffic within the terminal maneuvering area (TMA) of an airport implementing point merge (PM) procedures. We model realistic descent profiles and assume all the arrivals are performing the most fuel-efficient continuous descent operations.**

On example of a high-traffic hour at Oslo-Gardermoen airport, we demonstrate how our optimization framework can be adapted to a dual-runway environment with PM arrival procedures. We compare two scenarios: in the first, the aircraft are forced to strictly adhere to the PM systems, while in the second scenario, aircraft are allowed to use shortcuts within TMA. Evaluating the resulting arrival flight efficiency, we notice that the optimization does not significantly improve the performance in a fixed setting where aircraft are forced to adhere to the PM structure. Introducing some flexibility by allowing for direct routes from the intermediate waypoints, we can improve the overall performance, with the average fuel savings of 20% per flight, accompanied by the reduction of gaseous and particle emissions. [1]

***Keywords*—Arrival and Departure Scheduling, Point Merge, Continuous Descent Operations, Integer Programming**

I. Introduction

In a previous work [1], we presented the concept of automatic traffic scheduling in the Terminal Maneuvering Area (TMA) using Mixed Integer Programming (MIP) optimization, to facilitate more environmentally-friendly approaches in high-traffic scenarios with Point Merge (PM) arrival procedures. The purpose of the optimization framework is to allow execution of a Continuous Descent Operation (CDO) with all aircraft safely separated at all time, and serve as an arrival manager (AMAN) which automatically assigns each aircraft the optimal arrival route, considering the current arrival flow. In this paper, we demonstrate how our optimization framework can be extended to work in a dual-runway environment with mixed arriving and departing traffic. Additionally, we assess the potential benefits of combining PM with a more flexible arrival route structure, where aircraft may use shortcuts and deviate from the published arrival routes. We apply our methodology to the Norwegian airport of Oslo-Gardermoen (ENGM), where PM has been used since 2011, and compare our optimized arrival scenarios to the actual executed arrivals obtained from a historical open-access dataset.

The paper is organized as follows. In Section II, we review existing approaches to arrival optimization. In Section III, we describe our methodology, including the generation of arrival routes and descent profiles, setting up the optimization problem, and the metrics we use for the evaluation. In Section IV, we define a case study to which our optimization framework is applied, as well as present the obtained results. Finally, in Section VI, we provide our conclusions and proposal for future research.

II. Related Work

Automatic scheduling of flights in a PM environment was considered in [2], where the authors used an already proposed (but not yet implemented) PM layout for the Spanish airport of Palma de Mallorca, and designed an automation control tool. Their simulations showed that holding times could be reduced and that more aircraft would be able to fly CDOs. The authors of [3] proposed a novel PM design to the Chinese airport of Beijing Capital International, to which they applied an autonomous arrival management system, with the potential to handle an increased amount of traffic without more workload on controllers. The same authors extended their work from [3], and proposed a Multi-layer Point Merge (ML-PM) system for autonomous arrival management, and enhanced the previous studies by considering changes in flight altitude and speed [4]. In [5], a new-designed PM system was proposed to one runway at Amsterdam-Schiphol airport, controlled by a MIP-based arrival management system. Automatic traffic scheduling using MIP was also considered in [6], where it was applied with the goal to maximize the number of neutral CDOs for the trombone procedures at Frankfurt-Main airport. The authors of [7] proposed a MIP formulation for safely separated merging of flight flows into the TMA, in order to minimize the number of non-achievable Controlled Time of Arrivals (CTAs), applied to Paris Charles De-Gaulle airport. Another MIP-based approach for the generation of optimized arrival routes to enable CDOs for all arriving aircraft, was presented

[1]This research is a part of the ODESTA and ODESTA-PM projects, supported by the Swedish Transport Administration (Trafikverket) and in-kind participation of LFV.

in [8], where scenarios with a high-traffic demand resulted in infeasible solutions. In [9], the authors addressed the problem by adding a flexible arrival time window, meaning that aircraft could arrive within a given time window at the TMA entry point. This time-shift is generated by adjusting the en-route cruise speed. The work was extended in [10] with a detailed explanation of the concept of operations (CONOPS), where the methodology was successfully tested on several scenarios with different traffic levels. We applied similar methodology in [1], where MIP-based automatic traffic scheduling was considered for PM arrival procedures, including the integration of departing aircraft.

Other methods for improving the TMA performance include, for instance [11], where the authors show how the throughput can be increased in congested terminal airspace by deviating from the traditional first-come-first-served (FCFS) approach. In [12], the merging of traffic flows was studied, where the optimization of the aircraft trajectories merging at a given fix was done in two steps in order to ensure a sufficient separation between the arrival flows. In a more recent work, the authors of [13], presented various approaches to integrate several modelling features in the aircraft scheduling problem, for both departures and arrivals, with the aim of minimizing, for instance, the total travel time or maximum delay.

III. Methodology

This work is an implementation of the CONOPS, described in [10], and also implemented in [1], which enables four-dimensional trajectory negotiation/synchronization process between the Air Traffic Control Officer (ATCO) and the aircraft. This process is performed in the pre-sequencing area, while the aircraft are still in the en-route flight phase, and starts with arrival routes being generated by a ground support tool and then up-streamed to the aircraft. The Flight Management System (FMS) in the cockpit uses the arrival routes for constructing the optimal descent profiles, and the ground support tool will assign a route to each aircraft. The route assignment shall ensure that there is enough separation at any given waypoint that is being used by more than one aircraft. The optimized arrival routes allow the aircraft to fly neutral CDOs whenever descent is permitted (e.g. not along PM arcs). In addition, our framework ensures separation between the arrivals and the departures for optimized runway utilization in a dual-runway environment. As stated in Section I, the contributions to our existing optimization framework is the modification of the model to a dual-runway environment with two associated PMS, as well as introducing a more flexible scenario, where shortcuts may be assigned to aircraft. Moreover, we quantify the resulting arrival performance using a number of metrics including a couple of new indicators specifically designed for evaluation of the utilization of the PM procedures, as well as evaluating the emissions and noise levels.

A. Oslo-Gardermoen Airport

We apply our methodology to the Norwegian airport of Oslo-Gardermoen, handling 255.000 aircraft movements per year (2019) [14]. The airport operates with two parallel runways (01/19 L/R) that are used in either segregated or mixed mode. There are four PM systems in total (01 East and West, and 19 East and West), with overlapping sequencing legs at FL90, FL100 and FL110 in each system. The merge point of each system coincides with the initial approach fix (IAF) of the instrument landing system (ILS) procedure, for landing on either the left or the right runway.

B. Arrival Routes

We adjust the methodology described in [1], to optimize the arrivals to Oslo-Gardermoen airport runways 01 L/R, with two PM associated systems. A sketch of the published arrival routes for the six TMA entry points is presented in Figure 1. We use the Opensky Network database [15] to obtain trajectory data for historical flights within a 50 NM circle centered at the airport, for a certain time of interest. We analyze the historical trajectories of the flights and associate each flight to one of the six entry points, based on their direction of arrival. In practice, since the 50 NM circle does not contain five out of the six entry points, we find the intersection of the circle and the trajectory and save that as the initial point of the trajectory, and associate the flight with the nearest arrival route.

We are interested in arrival optimization for two different scenarios, where flights in the first scenario are strictly forced to follow the published arrival routes and are not allowed to shortcut, while flights in the second scenario may deviate from the published structure and make a direct route to one of the two merge points. The reason for the latter scenario is to allow aircraft to fly more efficient routes inside TMA, in case the traffic situation allows, since otherwise turning towards the merge point is possible only after reaching the Point Merge System (PMS). This flexibility contributes to the dynamic usage of the PM structure, combining the benefits of predictability and improved horizontal efficiency whenever possible. For the first scenario, this means that aircraft using the western PMS may turn towards the merge point only between the waypoint GM402 and the end of the arc, if coming from the north, and between the waypoint GM410 and the end of the arc, if coming from the south (Figure 2). The corresponding restriction for the eastern PMS is between GM403 and the end of the arc, and between GM416 and the end of the arc, for the northern and southern arrivals respectively. In the second scenario, with the shortcuts, we allow aircraft arriving via BELGU and INREX to turn directly towards the associated merge point already from one of the published waypoints (marked with green triangles in Figure 1). A shortcut is also allowed at the point where the flight enters the 50 NM circle.

Each arriving aircraft can be assigned one of the feasible routes, which differ in how long the aircraft stays on the sequencing leg of a PMS (or whether a shortcut is used or not, for flights from BELGU and INREX). We add two new equally-spaced waypoints in-between every pair of published waypoints along the sequencing legs, which results in six new points per arc and 24 new points in total, as shown in Figure 2.

The spacing between the points is between 1.7 and 2.2 NM, since the distance between the already published waypoints differs. This set, consisting of published and new waypoints, represent the points from which the aircraft will turn towards the corresponding merge point (INSUV or VALPU). We do not consider the final approach part of the arrival routes, hence, the arrival routes end at the intermediate approach fixes (IFs) NOSLA or OGRAS (Figure 2). Aircraft using the eastern PMS will go to merge point INSUV, while aricraft using the western PMS will go to merge point VALPU. From either of the two merge points, aircraft will fly towards NOSLA for an approach to runway 01R, or to OGRAS for an approach to runway 01L. Table I summarizes the total number of unique arrival routes available from each of the entry points. Each aircraft will follow one such route, which constitutes its horizontal profile.

TABLE I. NUMBER OF POSSIBLE ARRIVAL ROUTES PER ENTRY POINT, FOR THE TWO DIFFERENT SCENARIOS WITH AND WITHOUT SHORTCUTS

	ADOPI	BELGU	ESEBA	INREX	LUNIP	RIPAM
No shortcuts	11	11	11	11	10	10
Shortcuts	11	15	11	15	10	10

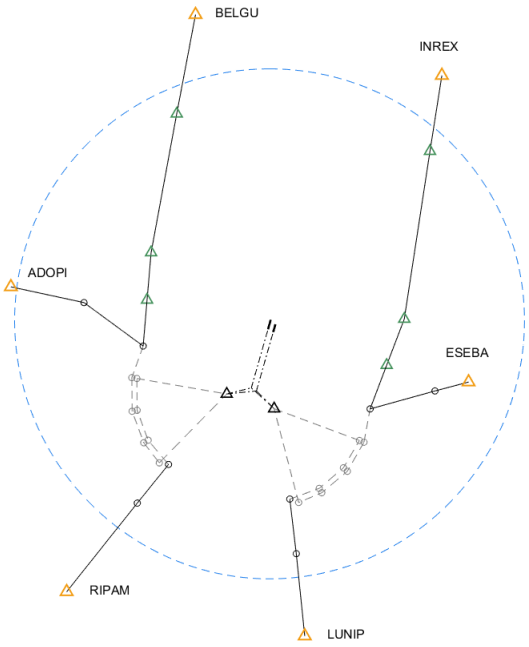

Figure 1. Fixed arrival route structure (solid lines) and variable PM segments (dashed line). Orange triangles depict the TMA entry points, while the green triangles represent the waypoints from which aircraft in the scenario with shortcuts may have a direct routing towards the merge points (black triangles). (source of data: Norwegian AIP [16]).

C. Vertical Profiles

For each horizontal profile, we create an associated vertical profile using EUROCONTROL Base of Aircraft DATA (BADA) v4.2 [17], that adhere to the restrictions valid for the published PM procedures at Oslo-Gardermoen airport. According to the corresponding chart from the Norwegian AIP [16], a speed restriction of max indicated airspeed (IAS) 220 kt applies to GM402, GM403, GM410 and GM416 (Figure 2). Moreover, GM410 and GM416 have a fixed altitude restriction of FL110, which shall be kept until the aircraft leaves the arcs and turns towards the merge point. For GM402, two aircraft may arrive simultaneously over the waypoint from two different arrival routes. This is possible since there is a fixed altitude restriction at GM402 of FL90 and FL100, respectively, for the two arrival routes. This means that the two aircraft are separated vertically by 1000 ft. Similar concept applies to waypoint GM403, connecting to the eastern PMS. We add an additional (not published) speed restriction of max IAS 200 kt over the two merge points, which we consider an operationally feasible restriction. In case the recommended speed in the speed profile for an aircraft type, provided in BADA, is lower than the speed restriction at any point during the descent, we set the speed to the value from BADA. Moreover, we match the initial IAS of the actual flight at entry to the 50 NM circle by setting the identical speed for the corresponding vertical profiles.

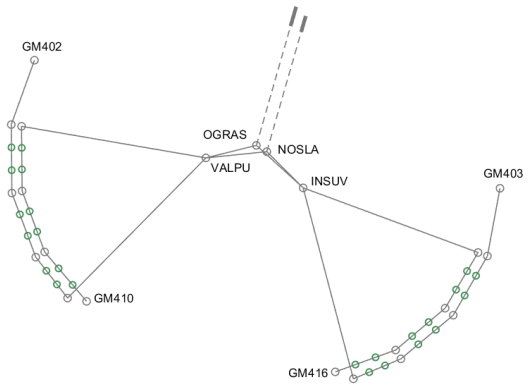

Figure 2. The two PMS for runways 01L/R of the Oslo-Gardermoen airport, with the additional waypoints depicted in green color, and the published waypoints in grey.

We model the vertical profiles with a 90% maximum landing weight, using the Total Energy Model (TEM) (Equation 1) to find the vertical speed (dh/dt). As long as the aircraft is descending, we assume an idle-thrust descent with no use of speedbreaks, with the thrust calculated from the BADA idle-rating coefficients. For level-flight segments, we set $dh/dt = 0$ and calculate the corresponding thrust. We obtain historical data on temperature and wind from the ECMWF [18] ERA5 reanalysis dataset, provided via the C3S Data Store. For further details on the modeling we refer to [1].

$$(Th - D) \cdot V_{TAS} = m \cdot g_0 \cdot \frac{dh}{dt} + m \cdot V_{TAS} \cdot \frac{dV_{TAS}}{dt} \quad (1)$$

D. Departing Aircraft

We account for departing aircraft by assigning them a departure time, when the takeoff-roll is initiated, based on data that we obtain from the Opensky Network database [15]. Since there is no good ground coverage in the data we use, the exact time of departure is not available, which we solve

by estimating the departure time based on time and position of the first recording, including a take-off roll of 30 sec.

E. Separation Requirements

1) Arrivals: The estimated capacity of a given runway system may be determined by considering the separation requirements enforced and the traffic mix, as proposed in [19]. In the book, the authors convert the separation requirements (given in nautical miles (NM)) to time, using a typical approach speed, depending on the Wake Turbulence Category (WTC) of the aircraft. The WTC combination of the leading and following aircraft in the pair, for which the required separation is to be determined, ultimately sets the separation requirement. The separation minima, as decided by the International Civil Aviation Organization (ICAO), are presented in Table II. The table also shows the proposed time-based separation from [19], which we use to define the necessary separation between two aircraft. We do not consider a reduced separation requirement when two aircraft are approaching simultaneously to the two parallel runways, i.e. in terms of separation, the runways are treated as one single.

TABLE II. RADAR SEPARATION MINIMA IN NM (SEC. IN PARENTHESIS)

		Trailing Aircraft		
		L	M	H
Leading Aircraft	L	2.5 (82)	2.5 (69)	2.5 (60)
	M	4.0 (131)	2.5 (69)	2.5 (60)
	H	6.0 (196)	5.0 (157)	4.0 (96)

2) Departures: The inclusion of the departing aircraft yields additional separation requirements. First, we need to make sure that any two aircraft depart with sufficient time in-between the initiation of their respective takeoff rolls. Furthermore, a landing aircraft may not touch down on the runway until a preceding departing aircraft has lifted off, and a departing aircraft may not initiate its takeoff roll until a preceding arriving aircraft has vacated the runway. We do not consider the inter-arrival/departure separation once the departing aircraft has lifted off from the runway.

F. Optimization Problem

1) Deconfliction: We initiate the optimization process by searching for incompatible profiles, i.e. identifying the profiles from different aircraft pairs that do not respect the required time separation at any given waypoint. Let $\mathcal{A}$ be the set of all aircraft scheduled to land at the airport during a certain period of time. Then, let $\mathcal{P}_a$ be the set of all feasible profiles for aircraft a, representing all possible arrival routes that aircraft a may follow along the published procedures. $\mathcal{I}$ represents the set of the aircraft-profile pairs (e.g. $((a_i, p_k), (a_j, p_r))$) containing the incompatibilities between profiles, meaning that there is a conflict between aircraft a_i and a_j if aircraft a_i flies profile p_k and aircraft a_j flies profile p_r, due to a loss of time-separation. The pseudocode in Algorithm 1, also used in [1], describes the deconfliction algorithm. In this paper, we have improved the performance of the code by only comparing aircraft profiles that possibly may interfere with each other, meaning that we exclude such comparisons where two profiles do not share a single common waypoint. In addition, in the case when two compared profiles use different arrival routes (belonging to different PMS), sharing only a one last waypoint, we use that information and compare only the time of arrival at the last waypoint. The conflict-pair constraint described in [1] still holds, assuring that at most one aircraft will be allowed to fly its profile in case there is an incompatibility between the two profiles. Allowing both profiles would result in a loss of separation. The deconfliction procedure also checks the separation within the arrival-time window, which we use to adjust the aircraft's time of entry to TMA, enabled by speed adjustments on cruise phase. We input the aircraft-profile pairs with incompatibilities into the optimization model, where the corresponding constraint ensures that the two conflicting profiles may not be selected simultaneously.

Algorithm 1 Deconfliction pre-processing step

```
for each pair of a/c do
  for i = 1 to #profiles of a/c 1 do
    for j = 1 to #profiles of a/c 2 do
      for k = 1 to #waypoints in profile i do
        for l = 1 to #waypoints in profile j do
          if i and j share a waypoint w then
            if difference in time at w < t_sep0 then
              mark the profile pair as conflicting
            end if
          end if
        end for
      end for
    end for
  end for
end for=0
```

2) MIP Setup: We seek to minimize the total transition time in TMA (TT), which is reflected in the objective function in Equation 2, formulated for the set of aircraft $\mathcal{A}$ and the set of profiles $\mathcal{P}_a$. In order to punish the selection of the profiles that have been time-shifted (i.e. the aircraft increased or decreased its speed during cruise), we add an extra hour (3600 sec.) to the time in TMA ($TT_{a,p}$) to the profiles shifted by $\pm$ 1 min. For profiles adjusted by more than 1 min., we keep adding the extra hour plus a couple of additional seconds. By doing so, we force the optimization to select a time-shifted profile only in case other solutions are infeasible. This will make the optimization prioritize a profile that has been shifted by the least amount of time.

$$\min \quad J := \sum_{a \in \mathcal{A}} \sum_{p \in \mathcal{P}_a} x_{a,p} \cdot TT_{a,p} \tag{2}$$

Equation 3 enforces that each aircraft is assigned only one profile, where the binary variable $x_{a,p}$ is set to 1 for the profile that is selected, for each unique arriving aircraft. Since the airport has multiple runways that may be used for landings, we need to add additional constraints and introduce a new binary variable for each runway in order to prevent the conflicts with

departing aircraft. Equations 4 and 5 set $x_{a,p}$ to the value of the corresponding binary variable for the individual runway, where $y_{a,p}$ is used for runway 01L and $z_{a,p}$ is used for runway 01R. The sets $\mathcal{P}_1$ and $\mathcal{P}_2$ contain the profiles for 01L/R runways, respectively. This set of constraints ensures that each aircraft is assigned only one profile and makes it possible to control that a landing aircraft does not interfere with a departure from the same runway. Note that the need for additional binary variables is required in order not to activate a separation constraint when a landing and a departing aircraft are using different runways, and would not be required if we would only consider the separation between arriving aircraft.

$$\sum_{p \in \mathcal{P}_a} x_{a,p} = 1, \quad \forall a \in \mathcal{A} \tag{3}$$

$$x_{a,p} = y_{a,p}, \quad \forall a \in \mathcal{A}, \forall p \in \mathcal{P}_1 \tag{4}$$

$$x_{a,p} = z_{a,p}, \quad \forall a \in \mathcal{A}, \forall p \in \mathcal{P}_2 \tag{5}$$

The binary variable $x_{a,p}$ is replaced either by $y_{a,p}$ or $z_{a,p}$, depending on whether the constraint is used for a departure from runway 01L or 01R, respectively.

G. Performance Metrics

In order to evaluate the performance of the optimized arrival flights, we use a set of metrics described in this subsection. We consider the parts of the aircraft trajectories starting from the point where the aircraft enters the 50 NM circle, until it reaches one of the two IFs (NOSLA or OGRAS).

1) Horizontal Flight Efficiency: We evaluate horizontal flight efficiency by assessing the distance flown by each aircraft within TMA.

2) Time in TMA: We assess the time in TMA by counting the time aircraft spend in TMA.

3) Vertical Flight Efficiency: We use the KPI of Time Flown Level to quantify the vertical efficiency by using a technique proposed by EUROCONTROL in [20] with small changes. We identify a level segment when the aircraft is descending with less than 300 feet per minute for at least 30 seconds, and do not consider these initial 30 seconds for the calculation. We do not consider the cruise phase a level segment (in case parts of the cruise is within the TMA), as it does not constitute a flight inefficiency, but rather a consequence of a low cruise altitude with the top of descent (ToD) being inside TMA.

4) PM Utilization: We quantify the utilization of PM by calculating to which extent (if any) the PM arcs are utilized by each aircraft, using the metric introduced in [21]. It is defined as the proportion of the length of the PM sequencing leg flown by the arriving aircraft to the full length of the sequencing leg. We use a small circular catching area of ≈2 NM around each waypoint along the arcs of the PMS, to identify via which waypoint the aircraft enters the system, and from which waypoint it leaves the arc.

5) Fuel Efficiency: We evaluate the fuel efficiency by calculating the fuel consumption according to the formula provided in the BADA manual. For the CDO part of the descent profile, we use the aircraft-specific idle thrust fuel coefficient, and for the part where additional thrust is required to maintain level-flight, we obtain the fuel coefficient via the thrust from Equation (1). We use the weather data source mentioned in Section III-C for the fuel calculation, i.e. [18].

6) Gaseous and Particle Emissions: We calculate the gaseous and particle emissions in terms of carbon dioxide (CO_2), nitrogen oxide (NOx), sulfur oxide (SOx), hydrocarbon (HC) and carbon monoxide (CO). For CO_2 and SOx, that depend linearly on the fuel burn, we use the factors 3.16 and 0.00084, respectively. For the remaining emissions, we apply IMPACT (3.37.D) tool [22], provided by EUROCONTROL, which we feed with the data on the aircraft's horizontal trajectory, altitude, true airspeed (TAS), corrected net thrust (adjusted for the ambient air pressure at the current altitude) and fuel flow. In IMPACT, we use the aircraft noise and performance (ANP) data v2.3 and the BADA versions 3.15 and 4.2, respectively. Furthermore, we consider the actual weather conditions for day of interest.

7) Noise: We use IMPACT for calculating the noise and provide the tool with the same input data as used for calculating the emissions, explained in Section III-G6. We perform the calculations based on ECAC.CEAC Doc 29 4th edition [23] with ANP data v2.3, and a fixed grid of resolution 0.048 NM in both the X and Y directions. For noise metric, we consider L_{den} (day-evening-night noise level), where a 5 dB penalty is added to flights between 19:00 and 23:00, and 10 dB is added to flights between 23:00 and 07:00. L_{den} corresponds to the sound pressure level averaged over the year [24].

IV. Experimental Evaluation

In this section, we demonstrate how to apply the proposed methodology on example of a high-traffic hour at Oslo-Gardermoen airport. Using a set of metrics, we compare the arrival performance of the actual historical flights and the resulting optimized trajectories.

A. Dataset

In order to find a suitable scenario to apply our optimization framework to, we use the historical database of Opensky Network [15]. We analyzed the Oslo-Gardermoen Opensky data for the year 2019 and identified the busiest hour as October 1, 05:00-06:00 UTC (07:00-08:00 local time). The local weather at the airport during this hour was a temperature of 2°C, air pressure of 990 hPa, relative humidity of 86% and a headwind of 2 kt. There were 41 arriving aircraft present in the TMA during the selected hour, out of which four of them are turboprop aircraft and the rest are propelled by jet engines. Two of the jet aircraft are WTC Heavy (H) and the rest WTC Medium (M). Given this set of aircraft, we use 69 sec. separation for an M or H aircraft following an M, and 157 sec. separation for an M following an H, as presented in Table II. Table III shows how the 41 arriving aircraft used the

respective TMA entry points, while Figure 3 (a) shows the actual trajectories of the 41 flights. We notice that about 70% of the arriving aircraft use the western PMS and the rest use the eastern PMS. There are 14 aircraft departing from 01L and three from 01R, all WTC M. We set a separation requirement of 90 sec. between two consecutive departures, representing a safe separation for WTC M aircraft, to which all departing aircraft in our scenarios belong. For the time windows, we use a ± 2 min. window for the arrivals, meaning that an arriving aircraft may speed up or slow down to reach the TMA 2 min. earlier or later, respectively, while for the departures we use a window that allows for a 2 min. delay.

TABLE III. NUMBER OF AIRCRAFT ENTERING VIA (OR CLOSE TO) THE RESPECTIVE SIX TMA ENTRY POINTS

PMS West			PMS East		
ADOPI	BELGU	RIPAM	ESEBA	INREX	LUNIP
7	16	6	6	3	3

B. Optimized Arrival Schedule

We solve our MIP using the Gurobi optimization solver installed on a powerful Tetralith server [25], utilizing Intel HNS2600BPB computer nodes with 32 CPU cores, 384 GB, provided by the National Academic Infrastructure for Supercomputing in Sweden (NAISS). In total, there are 4420 unique profiles for the scenario without shortcuts, while for the scenario with shortcuts, there are 5180 profiles. In order to allow all 41 arriving and 17 departing aircraft to be scheduled, one arriving aircraft was delayed by 1 minute by using TMA arrival time window. This result applies to both scenarios, with and without shortcuts. For the departing aircraft in the scenario without shortcuts, 11 aircraft had their takeoff time delayed, with a median of 12 sec. For the departing aircraft in the scenario with shortcuts, 11 aircraft had their takeoff time delayed, with a median of 20 sec.

Prior to performing the optimization, we run the deconfliction in Matlab (explained in Section III-F1), executed on the same machine as for the MIP. The deconfliction runs for $\sim$15 hours, but the MIP itself is solved within $\sim$15 seconds. Since the time window of ± 2 min was not used in full, the computational time could be reduced even further due to the possibility of reducing the number of profiles. Table IV shows the utilization or the two runways by the 41 arriving aircraft in the two optimization scenarios, and accoring to the actual historical trajectories.

TABLE IV. RUNWAY UTILIZATION

	01L	01R
Actual	20	21
Opt. no shortcuts	27	14
Opt. with shortcuts	25	16

C. Performance Evaluation

1) Time in TMA: The comparison of the time aircraft spend in TMA for the actual and optimized arrival flights is shown in Figure 5 (a) and in Table V. We observe that the optimized arrivals, strictly adhering to PM, spend longer time in TMA compared to the actual flights, while introducing shortcuts makes the time in TMA lower than the one for the actual flights. The results are in line with what one can observe by visual analysis of the trajectories in Figure 3, which clearly illustrates that the actual trajectories contain shortcuts and are shorter than the optimized trajectories without shortcuts.

2) Horizontal Flight Efficiency: The statistics for the distance in TMA metric, for the actual and optimized flights, are shown in Figure 5 (b), with the average values presented in Table V. We can see that the optimized arrivals forced to perform PM, tend to fly longer distances than the actual flights, while in the optimized scenario with the shortcuts, the resulting flown distances are identical to the ones of the actual flights. Hence, the optimized flight tracks are longer, but correspond to the shorter time in TMA, which can be explained by the difference in speed profiles.

3) Vertical Flight Efficiency: In Figure 4, we observe that the optimized trajectories, in general, are steeper than the real profiles. The vertical profiles of the optimized arrivals contain no level segments other than along the sequencing legs. However, there are a couple of very steep profiles shown in Figures 4 (b) and (c), which belong to turboprop aircraft. Using an idle-thrust descent for turboprop aircraft may result in too steep profiles, which we may solve by modeling a powered descent.

The results for the time flown level are summarized in Figure 5 (c) and Table V. We observe that both of the optimized scenarios have a greater time flown level compared to the actual flights, with the scenario without shortcuts having the largest, which may indicate that the sequencing legs are used more frequently by the optimized arrivals. The very long time flown level values in the two optimized scenarios, correspond to the turboprop aircraft that descend steeply (as explained above) which results in an extended level-flight segment before descending after leaving the sequencing legs.

TABLE V. AVERAGE TIME, DISTANCE, TIME FLOWN LEVEL AND FUEL BURN FOR THE ACTUAL TRAJECTORIES AND THE TWO SCENARIOS WITH OPTIMIZED TRAJECTORIES

	Average time [min]	Average distance [NM]	Average time flown level [%]	Average fuel burn [kg]
Actual	13.2	61.3	8.1	171.6
Opt. no shortcuts	14.3	66.7	23.5	191.3
Opt. with shortcuts	12.7	61.4	13.6	138.0

4) Fuel Efficiency: The distribution of the fuel consumption for the actual and optimized scenarios is shown in Figure 5 (d), with average values presented in Table V. We observe that strictly adhering to PM results in increased fuel consumption compared to the actual flights, while there is a significant decrease of 20% when allowing for shortcuts. Since time and distance in TMA is similar for the optimized scenario with shortcuts and the actual flights, and the time flown level is greater for the optimized scenario, we conclude that most of the fuel savings for the optimized arrivals with shortcuts can be attributed to factors such as better idle thrust CDO execution, prior to reaching the level-flight PM arcs and

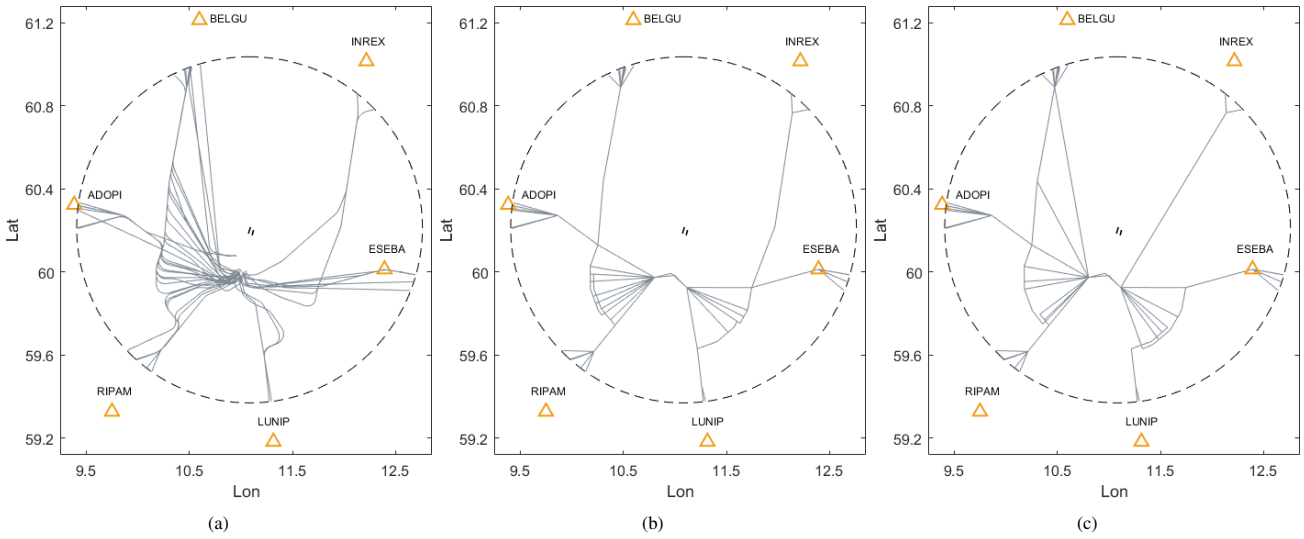

Figure 3. Actual trajectories (a), optimized trajectories without shortcuts (b) and optimized trajectories with shortcuts (c). The six TMA entry points are depicted as orange triangles, while the dashed circle represents the 50 NM radius centered at the airport.

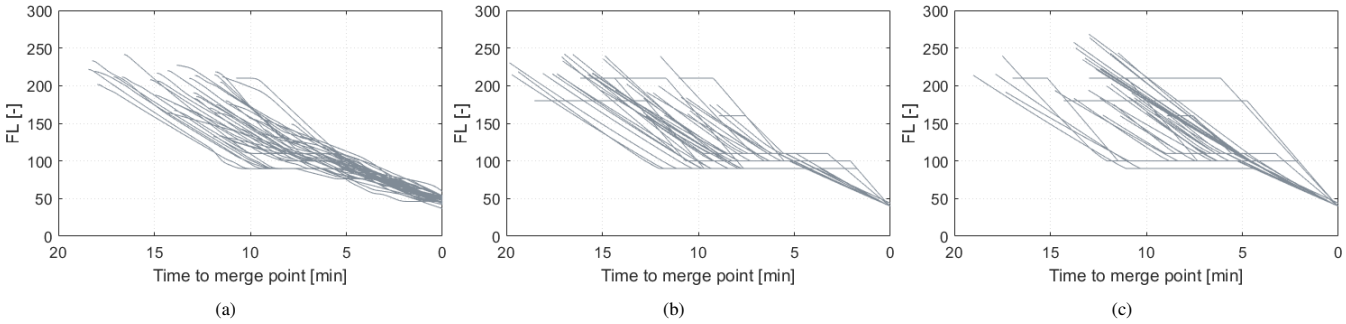

Figure 4. Vertical trajectories of the actual flights (a), optimized flights without shortcuts (b) and optimized flights with shortcuts (c).

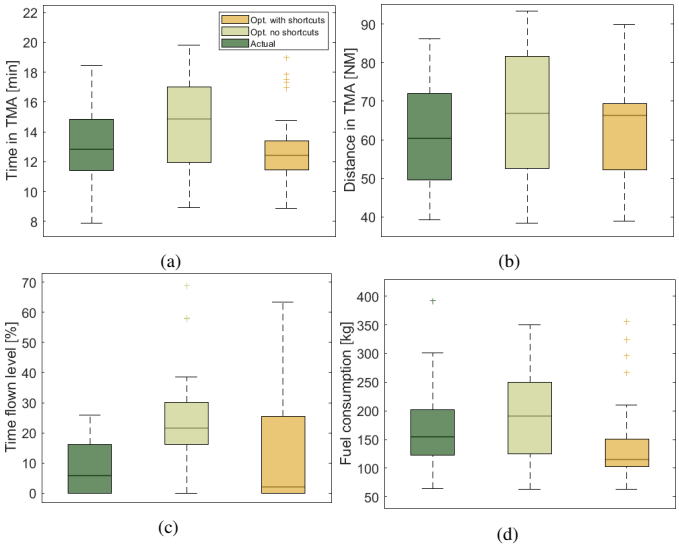

Figure 5. Time (a), distance (b), time flown level (c) and fuel consumption (d) for the actual trajectories and the two scenarios with optimized trajectories.

thereafter between the arcs and the merge point. The decent profiles of the optimized scenarios represent an ideal case which assumes a continuous idle thrust descent except along the PM arcs.

5) PM Utilization: We present the results for the PM Utilization in Table VI. ”No PM” means that the aircraft did not even pass the initial waypoint of a PMS, while ”No arc” means that the aircraft turned directly from the initial waypoint of a PMS to the merge point. The number of aircraft that do not use PM at all are lower or identical in the optimized scenarios compared to the actual flights, for both the Eastern and the Western PM systems. Interestingly, we notice that in the optimized scenario with shortcuts, the number of aircraft utilizing the full arc is greater, and in terms of fuel consumption, allowing for shortcuts still results in better fuel efficiency (Figure 5 (d) and Table V). The optimized scenario without shortcuts still contains flights not detected inside a PMS by our algorithm, due to the fact that waypoints GM402 and GM403 (from which the aircraft may fly towards the merge point) are not considered as part of the arcs.

6) Noise: The results of the noise calculations are presented in Figures 6 and 8. Figure 6 illustrates that the noise benefits

TABLE VI. PM UTILIZATION (IN NUMBER OF AIRCRAFT) FOR ACTUAL TRAJECTORIES AND OPTIMIZED TRAJECTORIES FLIGHTS

		No PM	No arc	1/3 arc	2/3 arc	Full arc
01 E	Actual	9	1	0	1	1
	Opt. no shortcuts	6	4	1	1	0
	Opt. with shortcuts	6	1	2	3	0
01 W	Actual	17	5	1	3	3
	Opt. no shortcuts	10	8	3	5	3
	Opt. with shortcuts	17	2	3	0	7

TABLE VII. AVERAGE EMISSIONS IN KG PER FLIGHT FOR THE THREE DIFFERENT SCENARIOS

	CO_2	NOx	SOx	HC	CO
Actual	542	1.27	0.17	0.38	6.61
Opt. no shortcuts	605	1.59	0.19	0.38	7.20
Opt. with shortcuts	436	1.01	0.14	0.36	6.72

of the two optimized scenarios are similar, compared to the actual flights, with the resulting decrease in the 30-40 dB areas. This may be explained by better CDO execution and the more uniform distribution of the trajectories, adhering to the published arrival routes. The reason why the areas exposed to the noise levels of 45 dB and 50 dB are larger, is that the actual aircraft fly at a higher altitude over the IFs, than the flights of the optimized trajectories, where the altitude was fixed to 4000 ft. Additionally, due to the lack of historical flight data along the final approach, noise is extrapolated by IMPACT along this segment and not based on actual trajectory data. The most northern noise pattern to the west of the final approach, for the actual trajectories in Figure 8 (a), is the result of a couple of flights performing curved RNP AR approaches.

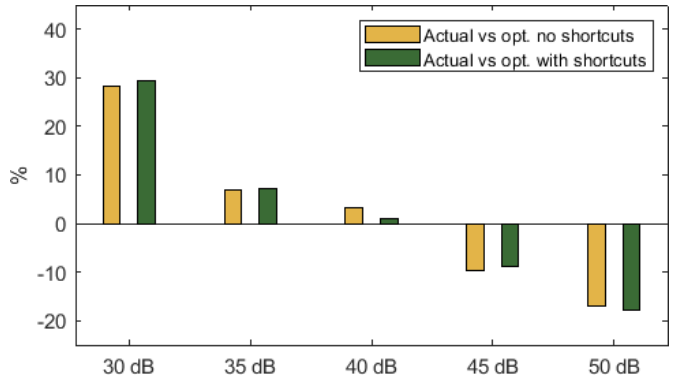

Figure 6. Additional areas exposed to noise of a certain level for the actual trajectories and the two scenarios with optimized trajectories.

7) Gaseous and Particle Emissions: Since the fuel burn for the optimized scenario without shortcuts is greater than for the actual trajectories, it follows that the emissions that depend linearly on the fuel consumption (CO_2 and SOx) also increase, as seen in Table VII. The corresponding results for NOx and CO are also higher, while for HC, the results are similar. All emissions studied here, except CO, are lower for the optimized scenario with shortcuts than the ones of the actual trajectories. The higher CO emissions may be explained by the increased idle-thrust operations, which is reported to produce higher levels of CO [26]. Figure 7 illustrates the emissions results.

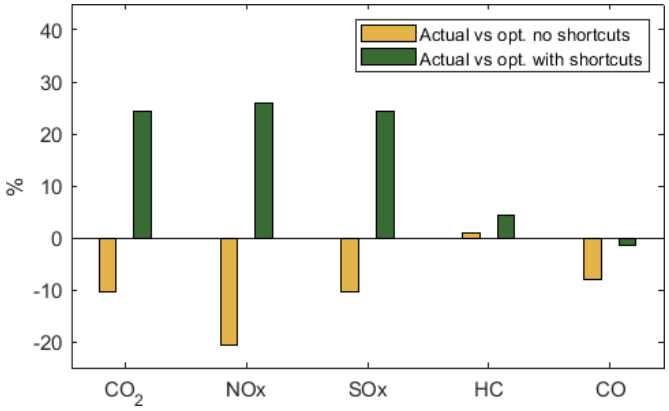

Figure 7. Additional emissions for the actual trajectories and the two scenarios with optimized trajectories.

8) Robustness: The optimization process assumes a perfect adherence by the aircraft to the assigned arrival route and the corresponding vertical profile. Factors such as, for example, different wind conditions (differing from what was used as input for the optimization framework), will alter the descent performance and ground speed of the aircraft. Adding some buffer time to the separation may be a solution to address such potential situations, which will unavoidably reduce the performance increment from the optimization. The corresponding robustness/performance trade-off is to be investigated further in future work.

V. CONCLUSION AND FUTURE WORK

In this paper, we present an application of the optimization framework for automated scheduling of arrivals performing energy-neutral descents within TMA, to the airport with two parallel runways and PM systems. We evaluate the results of the optimization applied to the arrivals to Oslo-Gardermoen airport during one high-traffic hour. We conclude that forcing the aircraft to adhere strictly to the PM procedures does not improve the arrival performance, while adding more flexibility by allowing for shortcuts from some of the published waypoints along the arrival procedures, we can increase the flight efficiency, with an average fuel savings of 20% per flight, in the given traffic situation and mix of aircraft types.

We plan to continue exploring the capabilities of our optimization framework, testing the settings where aircraft can fly to the alternative parts of the PMS in the event of bad weather obstructing the planned route, and also by adding more flexibility to departing aircraft, releasing the constraint of the fixed-runway assignment. The latter extension may also be complemented by controlling the balance in the runway usage. In order to further increase the operational feasibility of the framework, we consider modifying the model to improve robustness to the uncertainties of different types, as well as improving the computational complexity of the deconfliction process. In the future, the framework can serve evaluation of the airport capacity, in terms of the maximum number of aircraft successfully scheduled, by adding synthetic extra traffic into the schedule, until the demand meets the capacity.

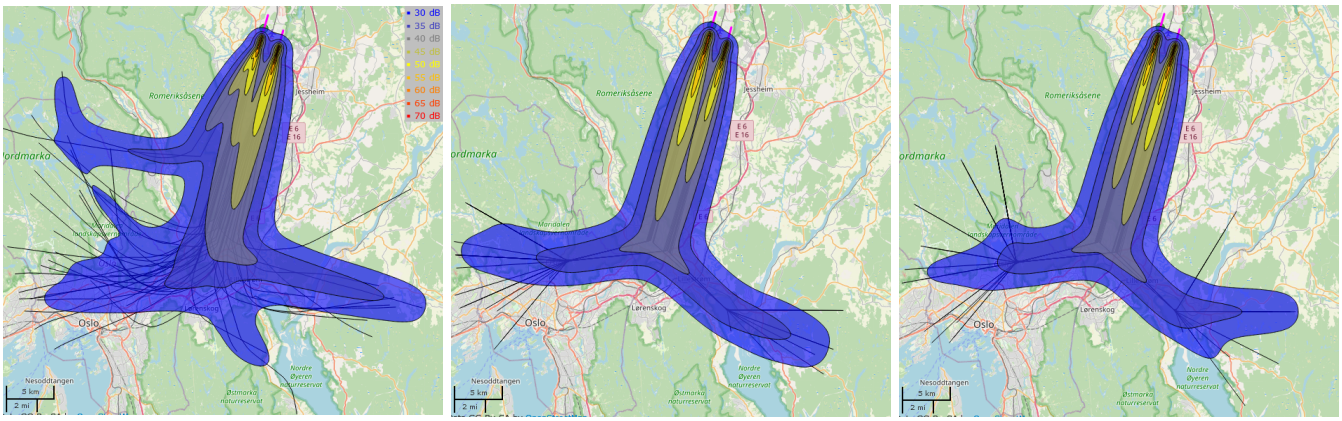

(a) (b) (c)

Figure 8. Noise contours for the levels 30-75 dB for actual trajectories (a), and optimized trajectories without shortcuts (b) and with shortcuts (c).

REFERENCES

[1] H. Hardell, T. Polishchuk, and L. Smetanová, "Automated Traffic Scheduling in TMA with Point Merge to Enable Greener Descents," in *ICRAT, Tampa, June 19-23, 2022*, 2022.

[2] L. S. Rebollar, "Automation Control of a Point Merge System at Palma de Mallorca airport," Bachelor's Thesis, UPC Barcelona, 2019.

[3] M. Liang, D. Delahaye, and P. Maréchal, "A Framework of Point Merge-based Autonomous System for Optimizing Aircraft Scheduling in Busy TMA," *5th SESAR Innovation Days, Bologna, Italy*, 2015.

[4] M. Liang, D. Delahaye, and P. Marechal, "Potential operational benefits of multi-layer point merge system on dense TMA operation - Hybrid arrival trajectory optimization applied to Beijing capital international airport," in *Proceedings of the 7th International Conference on Research in Air Transportation*, 2016.

[5] J. M. de Wilde, "Implementing point merge system based arrival management at Amsterdam Airport Schiphol," Master's Thesis, TU Delft, 2018.

[6] R. Sáez, X. Prats, T. Polishchuk, and V. Polishchuk, "Traffic Synchronization in Terminal Airspace to Enable Continuous Descent Operations in Trombone Sequencing and Merging Procedures: An Implementation Study for Frankfurt Airport," *TR-C: Emerging Technologies*, vol. 121, 2020.

[7] M. Sbihi, M. Mongeau, J. Ma, and D. Delahaye, "Merging Flows in Terminal Manoeuvring Areas via Mixed Integer Linear Programming," *GOW'16, XIII Global Optimization Workshop*, Sep 2016, Braga, Portugal, pp. 113-116; ISBN : 978-989-20-6764-3. hal-01379323.

[8] R. Sáez, S. Prats, T. Polishchuk, V. Polishchuk, and C. Schmidt, "Automation for Separation with CDOs: Dynamic Aircraft Arrival Routes," *AIAA Journal of Air Transportation*, vol. 28, no. 4, pp. 144–154, 2020.

[9] T. Polishchuk, V. Polishchuk, C. Schmidt, R. Saez, X. Prats, H. Hardell, and L. Smetanova, "How to Achieve CDOs for All Aircraft: Automated Separation in TMAs (Enabling Flexible Entry Times and Accounting for Wake Turbulence Categories)." in *SIDs*, 2020.

[10] R. Sáez, T. Polishchuk, C. Schmidt, H. Hardell, L. Smetanová, V. Polishchuk, and X. Prats, "Automated Sequencing and Merging with Dynamic Aircraft Arrival Routes and Speed Management for Continuous Descent Operations," *TR-C: Emerging Technologies*, vol. 132, 2021.

[11] S. Choi, J. E. Robinson, D. G. Mulfinger, and B. J. Capozzi, "Design of an optimal route structure using heuristics-based stochastic schedulers," in *IEEE/AIAA 29th DASC*, Oct. 2010.

[12] A. Michelin, M. Idan, and J. L. Speyer, "Mergin of Air Traffic Flows," *Journal of Guidance, Control and Dynamics*, vol. 34, no. 1, Feb 2011.

[13] M. Samà, A. D'Ariano, K. Palagachev, and M. Gerdts, "Integration methods for aircraft scheduling and trajectory optimization at a busy terminal manoeuvring area," *OR Spectrum*, vol. 41, pp. 641–681, Aug 2019.

[14] "Avinor," https://avinor.no/en/corporate/about-us/statistics/archive, last accessed on 05.02.2023.

[15] "Opensky Network," https://opensky-network.org/, last accessed on 11.02.2022.

[16] "Norwegian AIP," https://avinor.no/en/ais/aipnorway/, last accessed on 05.02.2023.

[17] EUROCONTROL, "User Manual for the Base of Aricraft Data (BADA) Family 4," 2014.

[18] "Copernicus Climate Change Service (C3S) Data Store, European Centre for Medium-Range Weather Forecasts (ECMWF)," https://cds.climate.copernicus.eu, last accessed on 11.02.2022.

[19] R. d. Neufville and A. R. Odoni, *Airport Systems*. Mc Graw Hill, 2013.

[20] EUROCONTROL, "Analysis of Vertical Flight Efficiency During Climb and Descent," 2017.

[21] H. Hardell, A. Lemetti, T. Polishchuk, and L. Smetanová, "Performance Characterization of Arrival Operations with Point Merge at Oslo Gardermoen Airport," in *ATM Seminar, Savannah, June 5-9, 2023*, 2023.

[22] EUROCONTROL, "IMPACT," https://www.eurocontrol.int/platform/integrated-aircraft-noise-and-emissions-modelling-platform, last accessed on 10.31.2022.

[23] ECAC, "ECAC.CEAC Doc 29 4th edition," 2016.

[24] "EASA," https://www.easa.europa.eu/eco/eaer/topics/adapting-changing-climate/noise, last accessed on 10.31.2022.

[25] "Tetralith server, NSC, Linköping University," https://www.nsc.liu.se/systems/tetralith/, last accessed on 11.02.2022.

[26] NASA, "Aircraft Particle Emissions eXperiment (APEX), NASA/TM—2006-214382," 2006.